PERGAMON

International Journal of Heat and Mass Transfer 42 (1999) 3771–3786

International Journal of HEAT and MASS TRANSFER

www.elsevier.com/locate/ijhmt

Semi-analytical solution for heat transfer from a buried pipe with convection on the exposed surface

Mo Chung[a, 1], Pyung-Suk Jung[a], Roger H. Rangel[b,*]

[a]*Department of Mechanical Engineering, Yeungnam University, 214-1 Dae-dong, Kyungsan 712-749, South Korea*
[b]*Department of Mechanical and Aerospace Engineering, University of California, Irvine, CA 92697-3975, USA*

Received 5 November 1998; received in revised form 30 January 1999

Abstract

The problem of heat transfer from a constant-wall-temperature pipe buried in a semi-infinite solid medium with a plane surface exposed to a fluid flow is solved semi-analytically. Using a conformal mapping, the original semi-infinite physical domain is transformed into a finite rectangular domain. A singular Fredholm integral equation of the second kind is derived and solved numerically to find the temperature distribution for the solid. The total heat flux Q from the exposed surface is expressed by modifying the conventional expression $Q=kS\Delta T$ to $Q=\eta kS\Delta T$, where S is the conduction shape factor, k is the thermal conductivity of the solid, and ΔT represents the temperature difference between the pipe wall and the surrounding fluid. The panel efficiency η and maximum surface temperature are presented in terms of the Biot number and a geometric parameter, L/D.

1. Introduction

Heat transfer from an isothermal circular pipe to a plane surface exposed to convective fluid motion (see Fig. 1) is a classical heat conduction problem with a wide range of practical applications. Pipes buried underground to carry water or oil are analyzed by many researchers to investigate the possibility of freezing of the fluid. In Asian countries, direct heating of residential floor by buried pipes (for example the *Ondol* system in Korea) is a popular form of space heating. The concept of conduction shape factor is widely used for steady-state heat transfer calculations associated with constant-wall-temperature buried pipes. The shape factor concept was introduced by Langmuir [1] and a large volume of data has been compiled for common geometrical configurations by Sunderland and Johnson [2] and Hahne and Grigull [3] among many authors. Most contemporary heat transfer textbooks, for example Bejan [4], Holman [5], Incropera and DeWitt [6], and Mills [7], devote a section on multi-dimensional steady heat transfer based on conduction shape factor.

The heat transfer rate for a multi-dimensional steady system, where only two temperature limits are involved, is calculated from

$$Q = kS\Delta T \tag{1}$$

where Q is the heat transfer rate per unit length, k is the thermal conductivity of the solid, and ΔT is the temperature difference between the two surfaces. The shape factor for a buried pipe is [4–7]

* Corresponding author. Tel.: +1-949-824-4033; fax: +1-949-824-8585.

E-mail address: rhrangel@uci.edu (R.H. Rangel)

[1] On leave at Department of Mechanical and Aerospace Engineering, University of California, Irvine, USA

0017-9310/99/$ - see front matter
PII: S0017-9310(99)00046-0

Nomenclature

a	pipe radius
Bi	the Biot number, Eq. (13)
a_0	leading Fourier cosines series coefficient
D	pipe diameter, $D=2a$
g	a function defined by Eq. (12)
h	step size for numerical integration
h_c	convective heat transfer coefficient
k	thermal conductivity of solid medium
L	distance between pipe center and ground surface, Fig. 1
Q	total heat transfer from ground surface per unit length
Q_{max}	maximum total heat transfer from ground surface per unit length
S	the conduction shape factor
T_a	ambient fluid temperature
T_w	pipe wall temperature
ΔT	$T_w - T_a$

Greek symbols

ϕ_0	a parameter defined by Eq. (7)
Φ	the unknown of integral equation, Eq. (17)
Γ	a geometrical parameter, L/a
γ	a parameter, $\sqrt{\Gamma^2-1}$
η	the panel efficiency, Eq. (29)
θ	normalized temperature, $(T-T_a)/\Delta T$

$$S=\frac{2\pi}{\cosh^{-1}(L/a)}. \tag{2}$$

One important restriction imposed on this shape factor formulation is that the surface of geometrical importance should be maintained at constant temperature. For buried pipe, this means that the convective heat transfer from the exposed surface is infinitely strong so that the fluid temperature and surface temperatures are the same. This restriction is obviously too strict for many practical applications. The purpose of this study is to investigate the effects of a finite heat transfer coefficient on the exposed surface on the heat transfer rate and temperature distribution, with the aim of providing a design criterion for heat transfer engineers.

2. Formulation

2.1. Assumptions

The following assumptions are made regarding the heat transfer process involving a buried pipe with a convective surface.

1. The process is steady.
2. The wall temperature of the pipe is uniform.
3. The convective heat transfer coefficient for the exposed surface is uniform across the surface.
4. The properties of the solid medium are constant.
5. The deep ground temperature is the same as the air temperature.

2.2. Governing equations

The governing equation for the conduction process is a Laplace equation. In terms of the dimensionless temperature, $\theta=(T-T_a)/(T_w-T_a)$, the energy equation becomes

$$\nabla^2\theta=\frac{\partial^2\theta}{\partial x^2}+\frac{\partial^2\theta}{\partial y^2}=0 \tag{3}$$

The boundary conditions are

1. Constant temperature condition, $\theta=1$, along the pipe wall.
2. Convective boundary condition, $h_c\theta(x,0)+k(\partial\theta/\partial y)\,|_{y=0}=0$, along the exposed surface.
3. Symmetry condition, $(\partial\theta/\partial x)\,|_{x=0}=0$, at the centerline.
4. Equilibrium temperature condition, $\theta\to 0$ as $x,\ y\to\infty$, far away from the tube.

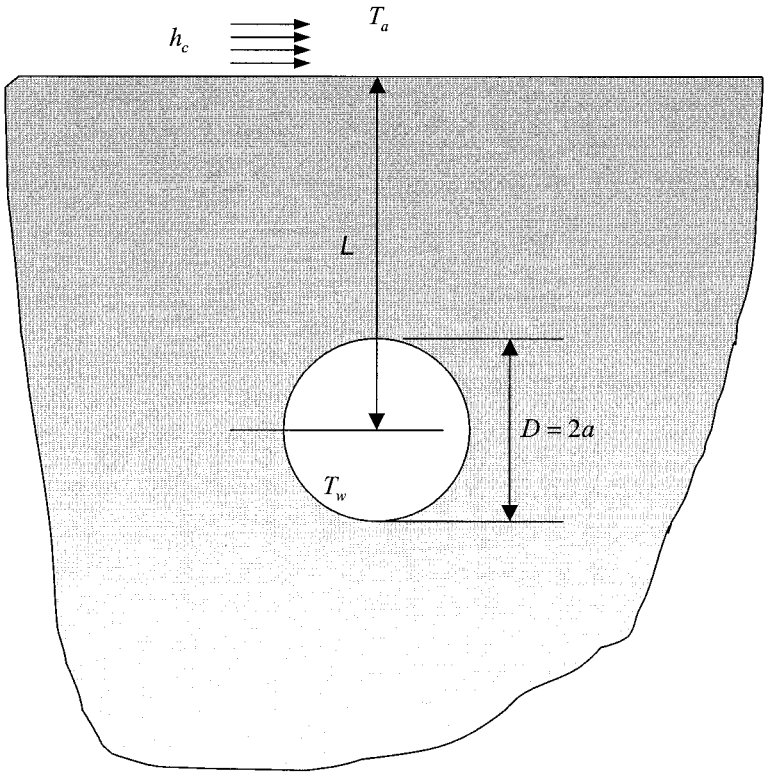

Fig. 1. Buried pipe with convective heat transfer from the exposed surface.

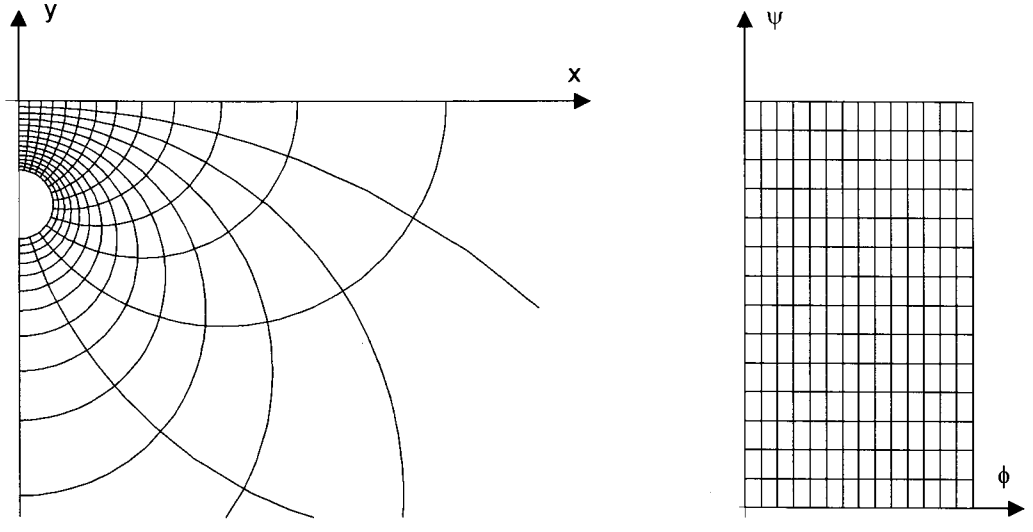

Fig. 2. Conformal mapping from physical domain to calculation domain [8].

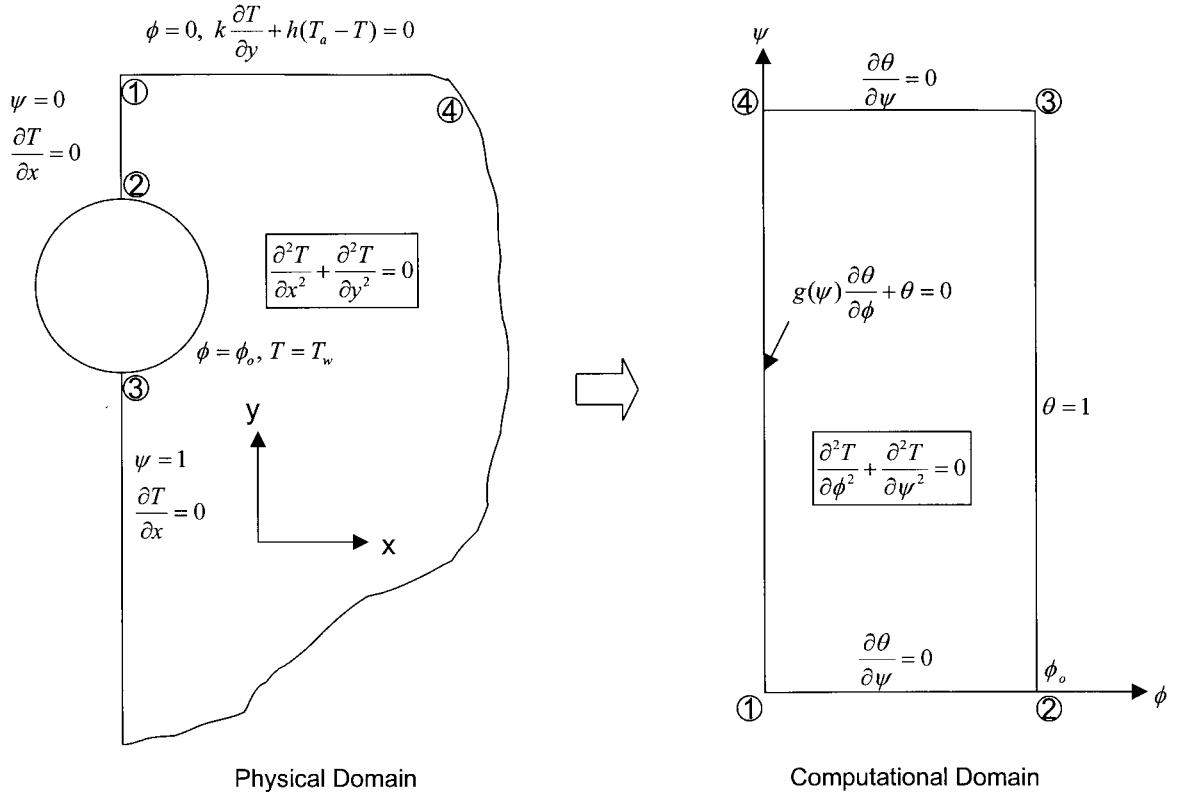

Fig. 3. Summary of governing equations and boundary conditions.

2.3. Coordinate transformation

The following conformal mapping is adopted to transform the physical domain into a simpler calculation domain [8]

$$\zeta = \phi + i\psi = F(z) = \frac{1}{\pi}\left[\ln\frac{iz + \sqrt{L^2 - a^2}}{iz - \sqrt{L^2 - a^2}}\right]. \tag{4}$$

The real and imaginary parts are

$$\phi(x, y) = \frac{1}{2\pi}\ln\left[\frac{x^2 + (y - \sqrt{L^2 - a^2})^2}{x^2 + (y + \sqrt{L^2 - a^2})^2}\right] \tag{5a}$$

$$\psi(x, y) = \frac{1}{\pi}\left[\tan^{-1}\left(\frac{x}{-y + \sqrt{L^2 - a^2}}\right) + \tan^{-1}\left(\frac{x}{y + \sqrt{L^2 - a^2}}\right)\right]. \tag{5b}$$

This transformation maps the semi-infinite physical domain onto a rectangle as shown in Fig. 2. The locations of various surfaces can be identified by the numbers in circle in Fig. 3. The parameter ϕ_0, which represents the size of the transformed domain, can be found from the mapping relation. The pipe wall is a circle whose equation is $x^2 + (y + L/a)^2 = 1$. The value of ϕ on the circle is constant and that value can be found

$$\phi_0 = \frac{1}{2\pi}\ln\frac{L + \sqrt{L^2 - a^2}}{L - \sqrt{L^2 - a^2}} \tag{6}$$

when the relation for the circle is substituted in the equation for ϕ, i.e. Eq. (5b). Alternatively, Eq. (6) may be written as [5]

$$\phi_0 = \frac{\cosh^{-1}(L/a)}{\pi} = \frac{2}{S}. \tag{7}$$

From a grid generation point of view, the conformal mapping not only produces a simple calculation domain but it also preserves the original form of the governing equation and the boundary conditions as will be shown below. This transformation also concentrates grid points near the top of the pipe where steeper gradients are expected.

The energy equation is transformed according to the following chain rules for partial derivatives:

$$T_x = T_\phi \phi_x + T_\psi \psi_x$$

$$T_y = T_\phi \phi_y + T_\psi \psi_y$$

$$T_{xx} = T_{\phi\phi}\phi_x^2 + 2T_{\phi\psi}\phi_x\psi_x + T_{\psi\psi}\psi_x^2 + T_\phi \phi_{xx} + T_\psi \psi_{xx}$$

$$T_{yy} = T_{\phi\phi}\phi_y^2 + 2T_{\phi\psi}\phi_y\psi_y + T_{\psi\psi}\psi_y^2 + T_\phi \phi_{yy} + T_\psi \psi_{yy}$$

Collecting terms for the original equation, a transformed energy equation can be obtained

$$\theta_{xx} + \theta_{yy} = (\phi_x^2 + \phi_y^2)\theta_{\phi\phi} + (\psi_x^2 + \psi_y^2)\theta_{\psi\psi} + 2(\phi_x\psi_x + \phi_y\psi_y)\theta_{\phi\psi} + (\phi_{xx} + \phi_{yy})\theta_\phi + (\psi_{xx} + \psi_{yy})\theta_\psi = (\phi_x^2 + \phi_y^2)(\theta_{\phi\phi} + \theta_{\psi\psi}).$$

The Cauchy–Riemann condition

$$\phi_x = \psi_y$$

$$\phi_y = -\psi_x$$

and the properties of a conformal mapping $\nabla^2\phi = 0$ and $\nabla^2\psi = 0$ are used in the above derivation. The energy equation in the transformed domain is further simplified to

$$\frac{\partial^2\theta}{\partial\phi^2} + \frac{\partial^2\theta}{\partial\psi^2} = 0 \tag{8}$$

since $\phi_x^2 + \phi_y^2$ is always positive for the calculation domain. Fig. 3 summarizes the governing equation and the boundary conditions for both domains.

2.4. Integral equation formulation

The transformed boundary conditions except for the convective boundary condition on the ground surface are of Sturm–Liouville type [9] owing to the coordinate alignment at the boundaries. The convective boundary condition at the ground surface before the transformation is

$$h_c\theta(x,0) + k\left.\frac{\partial\theta}{\partial y}\right|_{y=0} = 0. \tag{9}$$

Using the chain rule of differential calculus and the fact that $\partial\psi/\partial y = 0$ along the line $y = 0$ yield the following relationship at the ground surface

$$\frac{\partial\theta}{\partial y} = \frac{\partial\theta}{\partial\phi}\frac{\partial\phi}{\partial y} + \frac{\partial\theta}{\partial\psi}\frac{\partial\psi}{\partial y} = \frac{\partial\theta}{\partial\phi}\frac{\partial\phi}{\partial y}.$$

The metrics can be evaluated from the mapping relation

$$\left.\frac{\partial\phi}{\partial y}\right|_{y=0} = -\frac{2\sqrt{L^2 - a^2}}{\pi(x^2 + L^2 - a^2)} = \frac{-\cos\ \pi\psi - 1}{\pi a\sqrt{\Gamma^2 - 1}}$$

where the parameter

$$\Gamma = \frac{L}{a} \tag{10}$$

represents the geometric alignment of the pipe with respect to the exposed surface. In the above equation, the relation at the exposed surface

$$x = \sqrt{L^2 - a^2}\ \tan\left(\frac{\pi\psi}{2}\right)$$

is substituted to express the relation in terms of ψ. The top boundary condition is transformed to

$$\theta(0,\psi) + \frac{g(\psi)}{Bi}\left.\frac{\partial\theta}{\partial\phi}\right|_{\phi=0} = 0 \tag{11}$$

where the nondimensional function $g(\psi)$ is

$$g(\psi) = -\frac{1 + \cos\ \pi\psi}{\pi\sqrt{\Gamma^2 - 1}} \tag{12}$$

and Bi is the Biot number defined as

$$Bi = \frac{h_c a}{k_s}. \tag{13}$$

It is worth noting that the transformed boundary condition is not of Sturm–Liouville type because $g(\psi)$ is not constant. As a consequence, direct application of separation of variables based on orthogonal eigenfunctions is not viable.

In this study, an integral equation is derived from the convective boundary condition at the exposed surface. The first step is to construct the formal solution of the form

$$\theta(\phi,\psi) = a_0\left(1 - \frac{\phi}{\phi_0}\right) + \frac{\phi}{\phi_0} + \sum_{n=1}^{\infty} a_n\ \sinh\left[\lambda_n(\phi_0 - \phi)\right]\cos\ \lambda_n\psi. \tag{14}$$

This formal solution satisfies

1. The governing equation.
2. The boundary condition $\theta(\phi_0, \psi) = 1$ along the line of $\phi = \phi_0$.
3. $(\partial\theta/\partial\psi)|_{\psi=0} = 0$ along the lines of $\psi = 0$.
4. Fourier cosine series requirement of a leading constant a_0.

Applying the boundary condition along $\psi = 1$

$$\left.\frac{\partial\theta}{\partial\psi}\right|_{\psi=1}=0$$

yields the eigenvalues

$$\lambda_n = n\pi: \quad n=1,2\ldots \tag{15}$$

The only unknowns at this point are the coefficients a_n and one remaining condition is the boundary condition along the exposed surface, Eq. (11). As noted earlier, were the function $g(\psi)$ a constant, Eq. (11) could be used to find the coefficients a_n with the aid of the orthogonality properly associated with the eigenfunctions.

The integral equation is derived by satisfying Eq. (11). The partial derivative along the line $\phi=0$ of can be found from Eq. (14), namely,

$$\left.\frac{\partial\theta}{\partial\phi}\right|_{\phi=0}=\frac{1-a_0}{\phi_0}-\sum_{n=1}^{\infty}a_n\lambda_n\ \cosh\ \lambda_n\phi_0\ \cos\ \lambda_n\psi. \tag{16}$$

If the unknown function is defined

$$\Phi(\psi)\equiv\frac{1-a_0}{\phi_0}-\left.\frac{\partial\theta}{\partial\phi}\right|_{\phi=0}, \tag{17}$$

Eq. (16) can be expressed as

$$\Phi(\psi)=\sum_{n=1}^{\infty}a_n\lambda_n\ \cosh\ \lambda_n\phi_0\ \cos\ \lambda_n\psi.$$

Apparently, this is a typical Fourier cosine series except that $\Phi(\psi)$ is unknown. The coefficients a_n can be formally determined through Fourier cosine series

$$a_0=\int_0^1\theta(0,\xi)\,\mathrm{d}\xi \tag{18a}$$

$$a_n=\frac{2}{\lambda_n\ \cosh\ \lambda_n\phi_0}\int_0^1\Phi(\xi)\cos\ \lambda_n\xi\,\mathrm{d}\xi;\quad n=1,2,\ldots \tag{18b}$$

The boundary condition contains $\theta(0,\psi)$, which can be evaluated as

$$\begin{aligned}\theta(0,\psi)=&a_0+\sum_{n=1}^{\infty}a_n\ \sinh\ \lambda_n\phi_0\ \cos\ \lambda_n\psi\\ =&a_0+\sum_{n=1}^{\infty}\frac{2\ \tanh\ \lambda_n\phi_0}{\lambda_n}\\ &\times\int_0^1\Phi(\xi)\cos\ \lambda_n\xi\ \cos\ \lambda_n\psi\,\mathrm{d}\xi\\ =&a_0+\sum_{n=1}^{\infty}\frac{\tanh\ \lambda_n\phi_0}{\lambda_n}\int_0^1\Phi(\xi)[\cos\ \lambda_n(\psi-\xi)\\ &+\cos\ \lambda_n(\psi+\xi)]\,\mathrm{d}\xi.\end{aligned} \tag{19}$$

Substituting Eqs. (17) and (19) into (11) and changing the order of summation and integration yields a Fredholm integral equation of the second kind [10]

$$\begin{aligned}a_0+\int_0^1\Phi(\xi)\sum_{n=1}^{\infty}\frac{\tanh\ n\pi\phi_0}{n\pi}[\cos\ n\pi(\xi-\psi)\\ +\cos\ n\pi(\xi+\psi)]\,\mathrm{d}\xi+\frac{g(\psi)}{Bi}\left(\frac{1-a_0}{\phi_0}-\Phi(\psi)\right)=0.\end{aligned} \tag{20}$$

A point to note is that the infinite series in the kernel of the integral equation is not convergent because the sequence converges to $1/n$ (a harmonic series) as n increases to infinity where $\tanh n\pi\phi_0\to 1$. Based on the observation that the term $\tanh n\pi\phi_0$ rapidly converges to unity as n increases, the series is reorganized as a sum of two series (Kummer's transformation [11])

$$\begin{aligned}\sum_{n=1}^{\infty}\frac{\tanh\ n\pi\phi_0}{n\pi}\cos\ n\pi(\xi\pm\psi)=&\sum_{n=1}^{\infty}\frac{\cos\ n\pi(\xi\pm\psi)}{n\pi}\\ &+\sum_{n=1}^{\infty}\frac{\tanh\ n\pi\phi_0-1}{n\pi}\cos\ n\pi(\xi\pm\psi).\end{aligned}$$

The first sum on the RHS is added and subtracted in this manipulation. The first series on the right-hand side can be analytically summed and the second one is rapidly convergent as n increases. The function representation for first series is [12]

$$\sum_{n=1}^{\infty}\frac{\cos\ n\pi(\xi\pm\psi)}{n\pi}=-\frac{\ln[2\{1-\cos\ \pi(\xi\pm\psi)\}]}{2\pi}:$$

$$(0<|\ \xi\pm\psi\ |<2).$$

The kernel can be rewritten as

$$\begin{aligned}\sum_{n=1}^{\infty}\frac{\tanh\ n\pi\phi_0}{n\pi}&\quad[\cos\ n\pi(\xi-\psi)+\cos\ n\pi(\xi+\psi)]\\ =&-\frac{\ln[2\{1-\cos\ \pi(\xi-\psi)\}]}{2\pi}\\ &-\frac{\ln[2\{1-\cos\ \pi(\xi+\psi)\}]}{2\pi}\\ &-\sum_{n=1}^{\infty}\left\{\frac{1-\tanh\ n\pi\phi_0}{n\pi}\right.\\ &\left.\times[\cos\ n\pi(\xi-\psi)+\cos\ n\pi(\xi+\psi)]\right\}.\end{aligned}$$

The logarithmic singularity of this expression can be isolated utilizing the following series expansion

$$\frac{\ln[2\{1-\cos\ \pi(\xi+\psi)\}]}{2\pi}=\frac{\ln\ |\ \xi\pm\psi\ |}{\pi}+\ln\frac{\pi}{2}+\frac{\pi(\xi\pm\psi)^2}{24}+\frac{\pi^3(\xi\pm\psi)^4}{2880}+\frac{\pi^5(\xi\pm\psi)^6}{181{,}440}+O(\xi\pm\psi)^8. \tag{21}$$

The singular kernels can be reorganized as by isolating the singularities

$$\frac{\ln[2\{1-\cos\ \pi(\xi+\psi)\}]}{2\pi}=\frac{\ln\ |\ \xi+\psi\ |}{\pi}+\frac{\ln\ |\ \xi+\psi-2\ |}{\pi}+\left(\frac{\ln[2\{1-\cos\ \pi(\xi+\psi)\}]}{2\pi}-\frac{\ln\ |\ \xi+\psi\ |}{\pi}-\frac{\ln\ |\ \xi+\psi-2\ |}{\pi}\right)$$

and

$$\frac{\ln[2\{1-\cos\ \pi(\xi-\psi)\}]}{2\pi}=\frac{\ln\ |\ \xi-\psi\ |}{\pi}+\left(\frac{\ln[2\{1-\cos\ \pi(\xi+\psi)\}]}{2\pi}-\frac{\ln\ |\ \xi+\psi\ |}{\pi}\right).$$

The terms on the RHS of the above expressions are regular after the singularities are removed as can be seen from the series expansion, Eq. (21). The integral Eq. (20) can be conveniently written after singularities are isolated

$$\int_0^1 K_{\mathrm{S}}(\psi,\xi)\Phi(\xi)\,\mathrm{d}\xi+\int_0^1 K_{\mathrm{R}}(\psi,\xi)\Phi(\xi)\,\mathrm{d}\xi+\frac{g(\psi)}{Bi}\Phi(\psi)-\frac{g(\psi)}{Bi\phi_0}+a_0\left(\frac{g(\psi)}{Bi\phi_0}-1\right)=0 \tag{22}$$

where the singular kernel is

$$K_{\mathrm{S}}(\psi,\xi)=\frac{\ln\ |\ \xi-\psi\ |}{\pi}+\frac{\ln\ |\ \xi+\psi\ |}{\pi}+\frac{\ln\ |\ \xi+\psi-2\ |}{\pi} \tag{23}$$

and the regular kernel including the series parts is

$$K_{\mathrm{R}}(\psi,\xi)=\left\{\frac{\ln[2\{1-\cos\pi(\xi-\psi)\}]}{2\pi}-\frac{\ln\ |\ \xi-\psi\ |}{\pi}\right\}+\left\{\frac{\ln[2\{1-\cos\pi(\xi+\psi)\}]}{2\pi}-\frac{\ln\ |\ \xi+\psi\ |}{\pi}-\frac{\ln\ |\ \xi+\psi-2\ |}{\pi}\right\}+\sum_{n=1}^{\infty}\left\{\frac{1-\tanh\ n\pi\phi_0}{n\pi}\times[\cos\ n\pi(\xi-\psi)+\cos\ n\pi(\xi+\psi)]\right\}. \tag{24}$$

The remaining task is to express the constant a_0 in terms of the unknown function Φ. From the Fourier cosine series and the definition of $\Phi(\psi)$, Eq. (17), it is found that

$$a_0=\int_0^1\theta(0,\xi)\,\mathrm{d}\xi=-\int_0^1\frac{g(\xi)}{Bi}\frac{\partial\theta}{\partial\phi}\bigg|_{\phi=0}\mathrm{d}\xi=\int_0^1\frac{g(\xi)}{Bi}\Phi(\xi)\,\mathrm{d}\xi+\frac{a_0-1}{\phi_0 Bi}\int_0^1 g(\xi)\,\mathrm{d}\xi.$$

From this it follows that

$$a_0=\frac{1}{1+\pi\gamma\phi_0 Bi}+\frac{\pi\gamma\phi_0}{1+\pi\gamma\phi_0 Bi}\int_0^1 g(\xi)\Phi(\xi)\,\mathrm{d}\xi \tag{25}$$

where $\gamma=\sqrt{\Gamma^2-1}$. The following relation is used in the above derivation

$$\int_0^1 g(\xi)\,\mathrm{d}\xi=-\frac{1}{\pi\sqrt{\Gamma^2-1}}.$$

Replacing a_0 in Eq. (22), the integral equation can be finally written as

$$\int_0^1[K_{\mathrm{S}}(\psi,\xi)+K_{\mathrm{R}}(\psi,\xi)+K_{\mathrm{A}}(\psi,\xi)]\Phi(\xi)\,\mathrm{d}\xi+\frac{g(\psi)}{Bi}\Phi(\psi)=\frac{1+\pi\gamma g(\psi)}{1+\pi\gamma\phi_0 Bi} \tag{26}$$

where the kernel $K_{\mathrm{A}}(\psi,\xi)$ associated with is defined as

$$K_{\mathrm{A}}(\psi,\xi)=\frac{\pi\gamma[g(\psi)-\phi_0 Bi]}{1+\pi\gamma\phi_0 Bi}g(\xi). \tag{27}$$

2.5. Numerical solution of the singular integral equation

The numerical quadrature on a uniform mesh with arbitrary weight [13] is adopted to properly treat the integration involving the singular kernel. The numeri-

cal integration of a product of two functions, $w(x)$ and $f(x)$ is represented as a sum of a product of a weight and a function value over a four-point span as

$$\int_a^b w(\xi)f(\xi)\,\mathrm{d}\xi \cong \sum_{i=1}^{4} W_i f[(k+i-1)h]$$

where h is the step size. The weight factor is found by requiring the quadrature to be exact for 4 functions $f(x)=\text{const},\ x,\ x^2,\ x^3$

$$W_1 = \frac{1}{6}[(k+1)(k+2)(k+3)M_0 - (3k^2+12k+11)M_1 + 3(k+2)M_2 - M_3]$$

$$W_2 = \frac{1}{2}[-k(k+2)(k+3)M_0 + (3k^2+10k+6)M_1 - (3k+5)M_2 + M_3]$$

$$W_3 = \frac{1}{2}[k(k+1)(k+3)M_0 - (3k^2+8k+3)M_1 + (3k+4)M_2 - M_3]$$

$$W_4 = \frac{1}{6}[-k(k+1)(k+2)M_0 + (3k^2+6k+2)M_1 - 3(k+1)M_2 + M_3].$$

The moments of the weight function are given by

$$M_\mathrm{n} \equiv -\frac{1}{h^\mathrm{n}}\int_\mathrm{a}^\mathrm{b} \xi^\mathrm{n} w(\xi)\,\mathrm{d}\xi$$

and should be evaluated analytically over the same range of integration for a specific choice of $w(\xi)$. In this study, the weighting function $w(\xi)$ for the singular kernel is chosen in such a way as to suitably account for the logarithmic singularity

$$w(\xi) = K_\mathrm{S}(\psi,\xi)$$

$$f(\xi) = \Phi(\xi).$$

The moments of the weighting function for this choice are

$$M_0 = \int_\psi^\xi \log(\psi - t)\,\mathrm{d}t = [\log(\psi-\xi)-1](\psi-\xi)$$

$$M_1 = \int_\psi^\xi t\,\log(\psi - t)\,\mathrm{d}t = \frac{1}{4}(\psi-\xi)[-3\psi-\xi+2(\psi+\xi)\log(\psi-\xi)]$$

$$M_2 = \int_\psi^\xi t^2\,\log(\psi - t)\,\mathrm{d}t = \frac{1}{18}[-11\psi^3+6\psi^2\xi+3\psi\xi^2+2\xi^3 + 6(\psi^3-\xi^3)\log(\psi-\xi)]$$

$$M_3 = \int_\psi^\xi t^2\,\log(\psi - \xi)\,\mathrm{d}t = \frac{1}{48}[-25\psi^4+12\psi^3\xi+6\psi^2\xi+4\psi\xi^3+3\xi^4 + 12(\psi^4-\xi^4)\log(\psi-\xi)].$$

Most of mathematical analysis including the analytic integration for the moments are performed using symbolic software [14]. The numerical integration involving the regular kernel is carried out by splitting the integrand as a product of

$$w(\xi) = 1$$

$$f(\xi) = K_\mathrm{R}(\psi,\xi)\Phi(\xi).$$

This is equivalent to Simpson's 3/8 rule that has an accuracy of $O(h^5)$ and gives the following simple expressions for W_is

$$W_1 = \frac{3h}{8},\quad W_2 = \frac{9h}{8},\quad W_3 = \frac{9h}{8},\quad W_4 = \frac{3h}{8}$$

where h is the step size. Since Φ is not known, the integral Eq. (26) results in a system of linear simultaneous equations when the numerical quadrature scheme is applied

$$A_{ij}\Phi_j = b_i$$

where A_{ij} is an $n\times n$ matrix and b_j is a vector.

3. Results and discussion

3.1. Numerical performance

Two most important questions regarding the numerical solution of the Weakly Singular Integral Equation (WSIE), Eq. (26), are

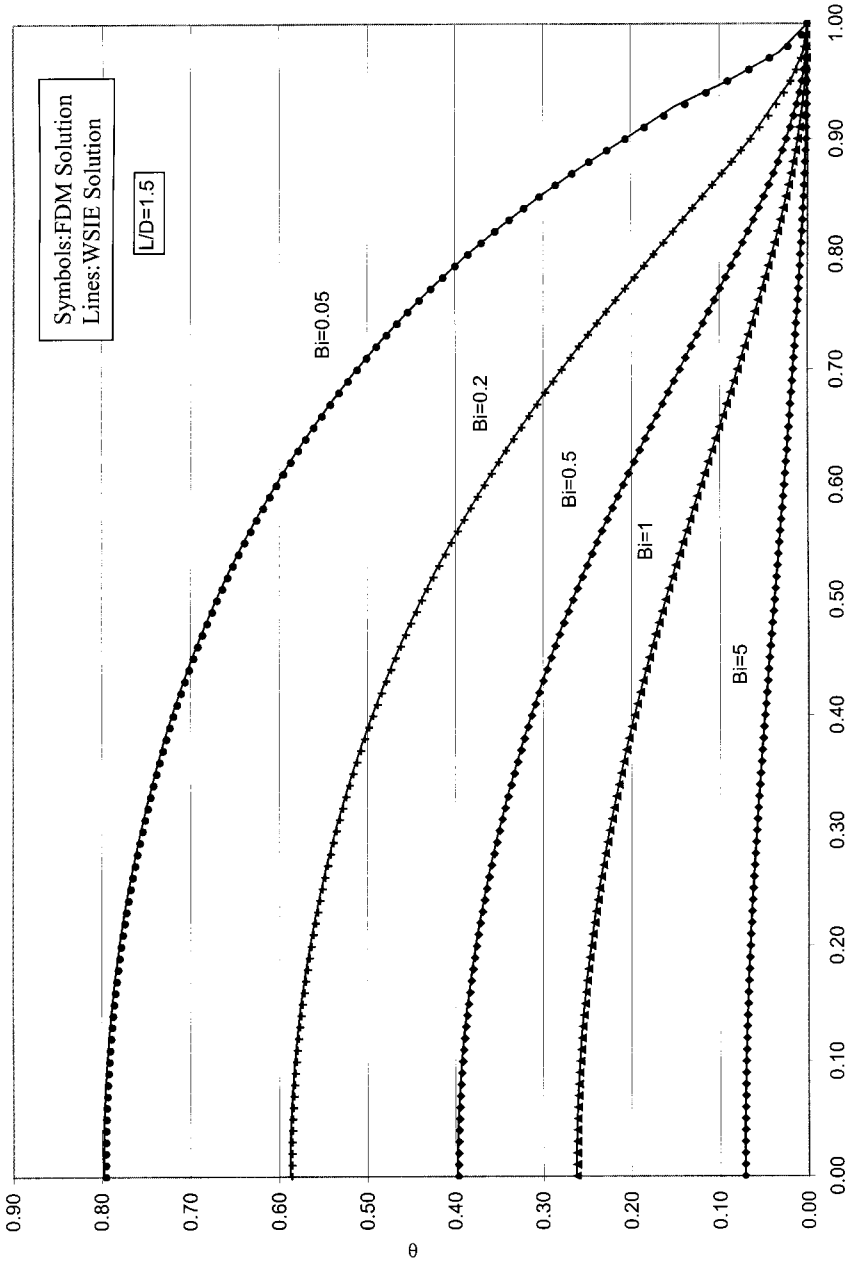

Fig. 4. Comparison of numerical solutions by FDM and WSIE.

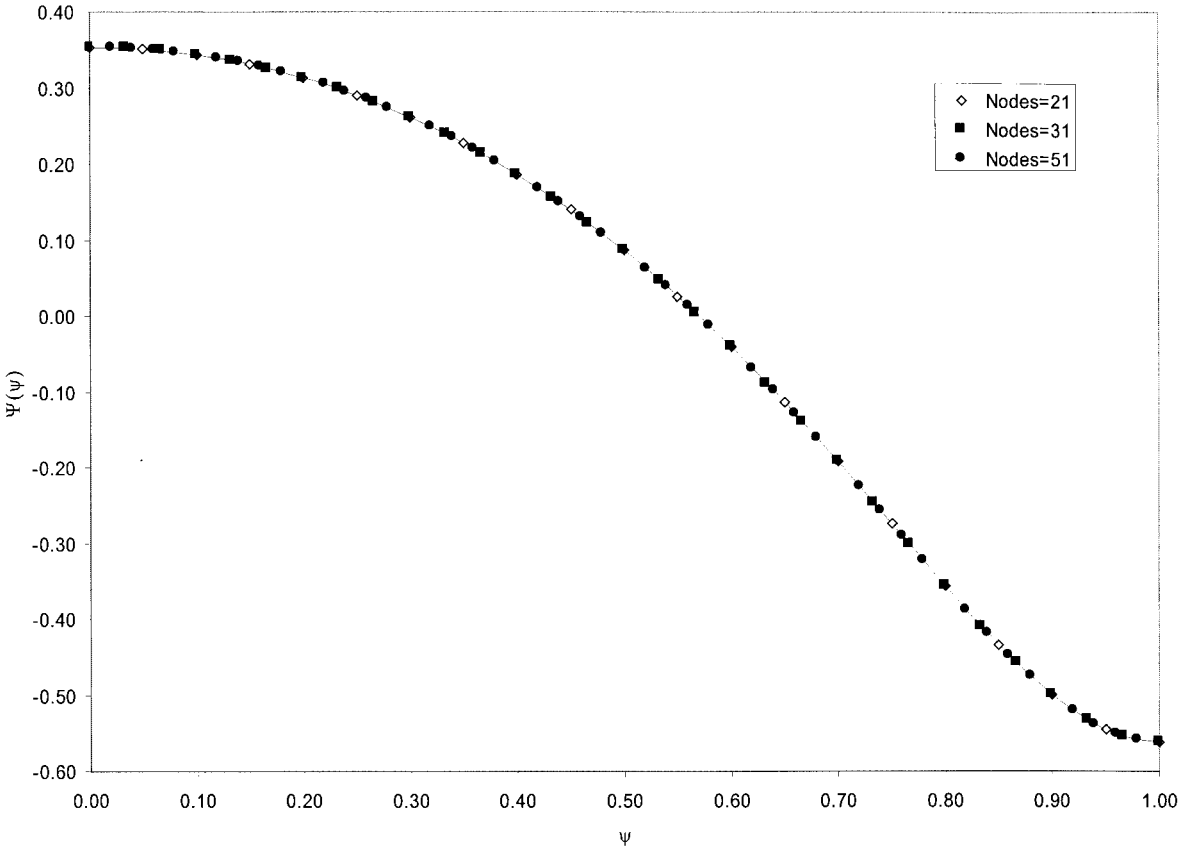

Fig. 5. Grid point convergence characteristics for numerical solution of WSIE.

1. Does the solution of the WSIE represent the physical problem correctly?
2. Is the numerical scheme reliably robust?

The best way to answer the first question is to find the solutions by independent methods and to compare them. For this purpose, the energy equation was directly solved in the transformed computational domain (see Fig. 3) using an Alternating Direction Implicit (ADI) based Finite Difference Method (FDM) for a verification of consistency. Actually, the FDM is a good alternative solution method because the numerical task is relatively simple on the transformed domain. Fig. 4 shows the temperature distribution on the exposed surface in terms of transformed coordinates for various Biot numbers. The symbols represent the FDM solution and the lines represent the WSIE solution. The agreement between the two solutions is very good. In the FDM solution, a 100×60 grid system is used and 1000–2000 ADI iterations are required to reach the maximum iteration error of 10^{-6}. For the same order of grid size, the CPU time for FMD was more than 10 times that for SIE. The answer to the second question can be found by a grid point convergence test. Fig. 5 shows the convergence characteristics of the numerical solution of the WSIE as a function of the number of grid points. The number of grid points tested are 21, 31, and 51 and the grid point convergence is very good. The Biot number is 1 and $L/D=3$ for this particular test. Another advantage of using the WSIE solution is the convenience of post processing. In the WSIE solution, the temperature distribution and heat flux on the exposed surface at arbitrary location can easily be evaluated once the function $\Phi(\psi)$ is found from the solution of the integral equation whereas the FDM solution needs interpolation. Calculation results for the physical quantities of interest such as the temperature distribution and heat flux distribution along the exposed surface, maximum temperature on the surface are discussed in the next section.

3.2. Total heat transfer rate form the surface

The total heat transfer rate from the ground surface to the surrounding can be found by integration of the

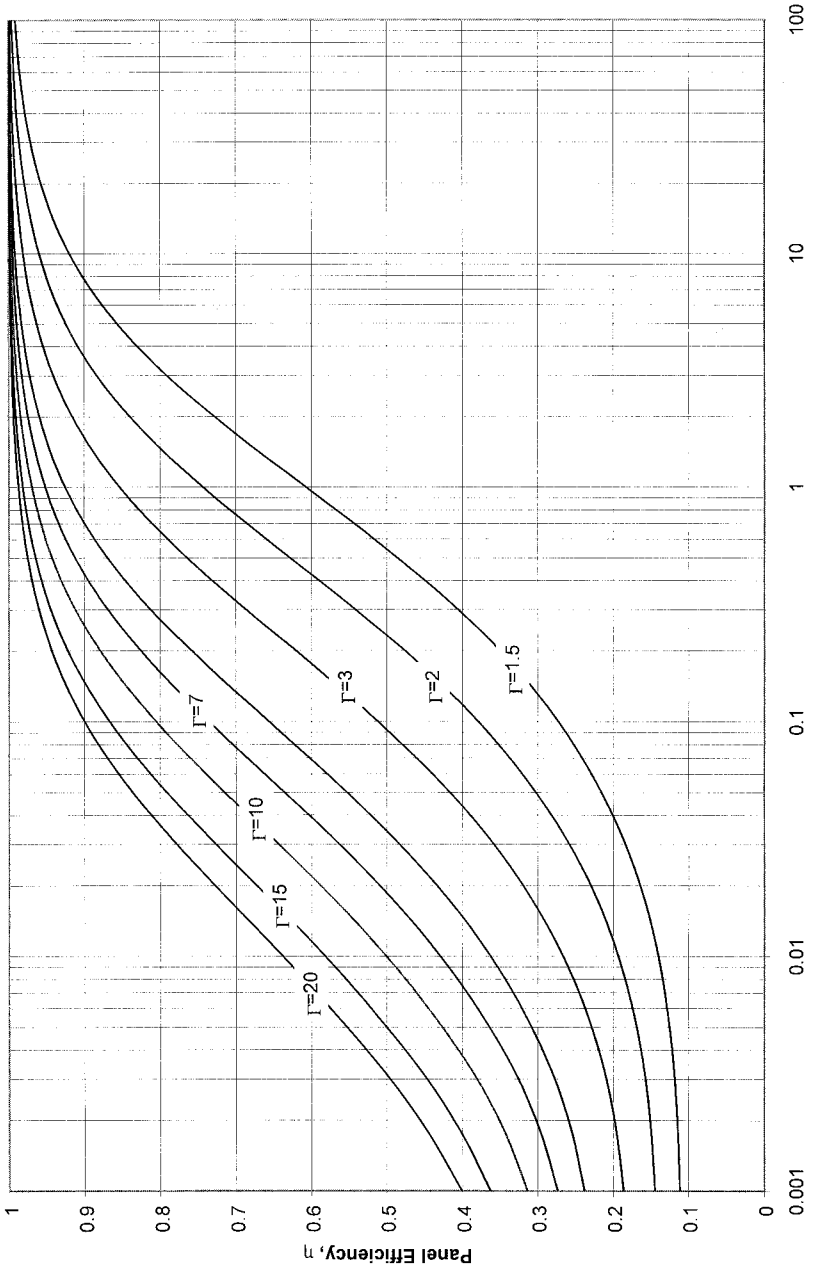

Fig. 6. Panel efficiency curves.

Table 1
Panel efficiency

	Γ												
Bi	1.5	2	3	4	5	6	8	10	12	14	16	18	20
0.001	0.111	0.144	0.186	0.215	0.238	0.257	0.288	0.313	0.335	0.354	0.371	0.386	0.400
0.01	0.140	0.193	0.266	0.320	0.362	0.398	0.456	0.500	0.537	0.568	0.594	0.617	0.638
0.05	0.215	0.302	0.416	0.494	0.553	0.598	0.666	0.715	0.751	0.779	0.802	0.821	0.836
0.1	0.272	0.379	0.511	0.596	0.656	0.701	0.763	0.805	0.835	0.857	0.874	0.888	0.899
0.2	0.350	0.476	0.620	0.704	0.758	0.797	0.847	0.879	0.900	0.915	0.927	0.935	0.943
0.3	0.405	0.541	0.686	0.764	0.812	0.845	0.886	0.911	0.928	0.939	0.948	0.955	0.960
0.5	0.486	0.628	0.764	0.830	0.869	0.894	0.925	0.942	0.953	0.961	0.967	0.971	0.975
1	0.607	0.743	0.853	0.900	0.925	0.941	0.959	0.969	0.975	0.980	0.983	0.985	0.987
1.5	0.680	0.803	0.893	0.929	0.947	0.959	0.972	0.979	0.983	0.986	0.988	0.990	0.991
2	0.728	0.840	0.916	0.944	0.959	0.968	0.978	0.984	0.987	0.990	0.991	0.992	0.993
3	0.791	0.883	0.941	0.962	0.972	0.978	0.985	0.989	0.991	0.993	0.994	0.995	0.996
4	0.830	0.908	0.954	0.971	0.979	0.984	0.989	0.992	0.994	0.995	0.996	0.996	0.997
5	0.856	0.924	0.963	0.976	0.983	0.987	0.991	0.993	0.995	0.996	0.996	0.997	0.997
6	0.876	0.935	0.969	0.980	0.986	0.989	0.993	0.995	0.996	0.997	0.997	0.997	0.998
7	0.891	0.944	0.973	0.983	0.988	0.991	0.994	0.995	0.996	0.997	0.997	0.998	0.998
8	0.902	0.950	0.976	0.985	0.989	0.992	0.994	0.996	0.997	0.997	0.998	0.998	0.998
10	0.919	0.959	0.981	0.988	0.991	0.993	0.996	0.997	0.997	0.998	0.998	0.999	0.999
25	0.965	0.983	0.992	0.995	0.997	0.997	0.998	0.999	0.999	0.999	0.999	0.999	1.000
50	0.982	0.991	0.996	0.998	0.998	0.999	0.999	0.999	1.000	1.000	1.000	1.000	1.000
75	0.988	0.994	0.997	0.998	0.999	0.999	0.999	1.000	1.000	1.000	1.000	1.000	1.000
100	0.991	0.996	0.998	0.999	0.999	0.999	1.000	1.000	1.000	1.000	1.000	1.000	1.000

local heat flux over the entire exposed surface

$$Q = \int_{-\infty}^{\infty} -k\frac{\partial T}{\partial y}\bigg|_{y=0} \mathrm{d}x$$

$$= -k\Delta T\int_{-1}^{1} g(\psi)\frac{\partial \theta}{\partial \phi}\bigg|_{\phi=0}\frac{\partial x}{\partial \psi}\bigg|_{y=0} \mathrm{d}\psi$$

$$= 2k\Delta T\int_{0}^{1} \frac{\partial \theta}{\partial \phi}\bigg|_{\phi=0} \mathrm{d}\psi. \tag{28}$$

The following mapping relation is used here

$$\frac{\partial x}{\partial \psi}\bigg|_{\phi=0} = -\frac{\partial y}{\partial \phi}\bigg|_{y=0} = -\frac{1}{g(\psi)}.$$

The total heat transfer from the exposed surface can be expressed in a convenient form for design purposes. Eq. (28) can be rearranged in terms of the shape factor

$$Q = 2k\Delta T\int_{0}^{1}\left(\frac{1-a_0}{\phi_0} - \Phi(\psi)\right)\mathrm{d}\psi$$

$$= kS\Delta T\left(1 - a_0 - \phi_0\int_{0}^{1}\Phi(\psi)\,\mathrm{d}\psi\right).$$

It will be useful to define a panel efficiency that compares actual heat transfer with that for the case where the surface temperature is constant

$$\eta = \frac{Q}{Q_{\max}} = \frac{Q}{kS\Delta T} = 1 - \left(a_0 + \frac{2}{S}\int_{0}^{1}\Phi(\psi)\,\mathrm{d}\psi\right). \tag{29}$$

Next, the total heat transfer rate is conveniently recast as

$$Q = \eta kS\Delta T. \tag{30}$$

Physically, the panel efficiency represents the ratio of actual heat transfer rate to the maximum possible heat transfer rate, which is attained when the Biot number is infinity. The panel efficiency, η, is a function of the Biot number and the geometric parameter L/D. Fig. 6 shows the efficiency curves as functions of the Biot number for different values of L/D. The panel efficiency is a strong function of both the Biot number and L/D and asymptotically approaches unity as the Biot number becomes large regardless of the value of L/D. Table 1 summarizes the numerical values of the panel efficiency.

3.3. Surface temperature distribution

In many applications such as panel heating systems, the temperature distribution on the exposed surface is very important because it is the primary factor that affects human comfort. The temperature distribution on the exposed surface can be found through Eqs. (11) and (17)

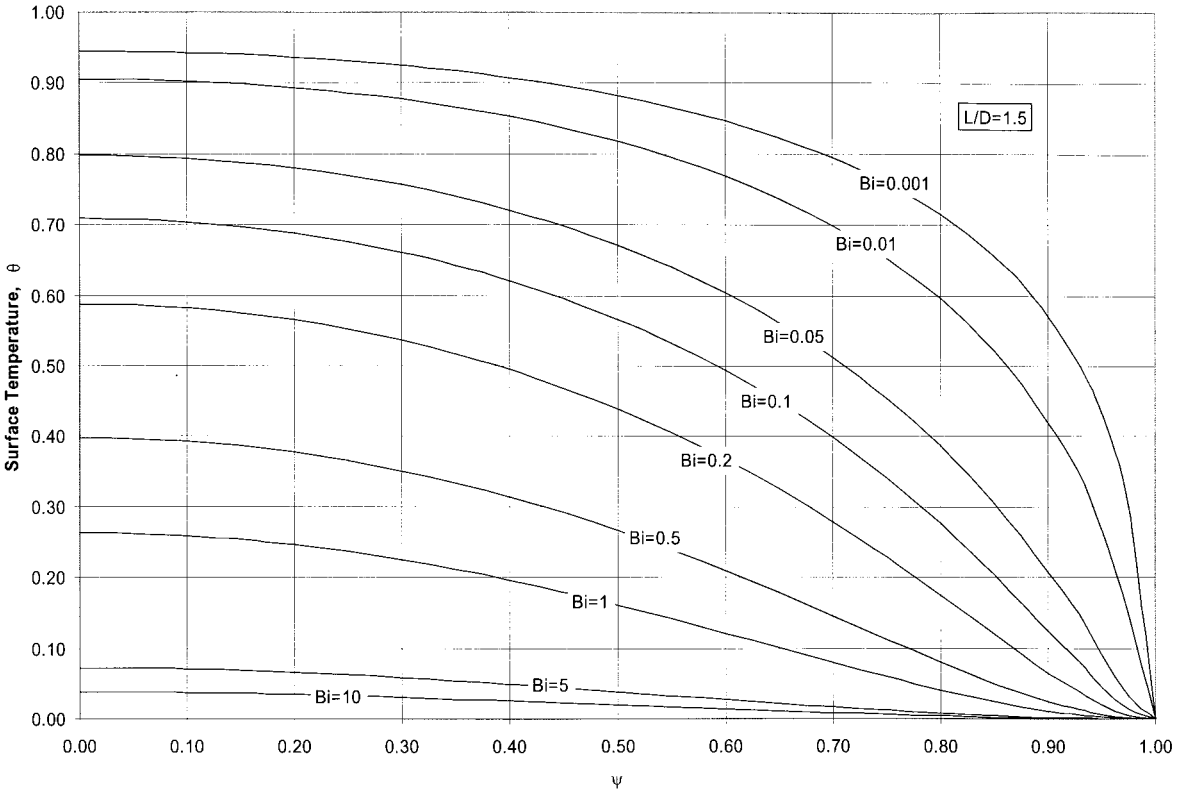

Fig. 7. Biot number effect on surface temperature.

Table 2
Maximum surface temperature

	Γ												
Bi	1.5	2	3	4	5	6	8	10	12	14	16	18	20
0.001	0.994	0.977	0.945	0.918	0.896	0.877	0.847	0.822	0.800	0.781	0.765	0.749	0.735
0.01	0.987	0.960	0.905	0.857	0.816	0.781	0.721	0.673	0.633	0.598	0.567	0.540	0.516
0.05	0.961	0.904	0.798	0.714	0.646	0.591	0.505	0.441	0.392	0.352	0.320	0.293	0.271
0.1	0.932	0.848	0.709	0.606	0.529	0.469	0.382	0.321	0.277	0.243	0.216	0.194	0.176
0.2	0.881	0.761	0.588	0.475	0.397	0.340	0.263	0.213	0.178	0.153	0.133	0.118	0.106
0.3	0.836	0.693	0.506	0.394	0.320	0.269	0.202	0.160	0.132	0.112	0.097	0.085	0.076
0.5	0.761	0.591	0.398	0.295	0.233	0.191	0.139	0.108	0.087	0.073	0.063	0.055	0.048
1	0.625	0.436	0.263	0.184	0.140	0.112	0.078	0.060	0.048	0.040	0.034	0.029	0.026
1.5	0.532	0.347	0.197	0.134	0.100	0.079	0.055	0.041	0.033	0.027	0.023	0.020	0.017
2	0.463	0.288	0.158	0.106	0.078	0.061	0.042	0.032	0.025	0.021	0.017	0.015	0.013
3	0.369	0.216	0.113	0.074	0.054	0.042	0.029	0.021	0.017	0.014	0.012	0.010	0.009
4	0.307	0.173	0.088	0.057	0.042	0.032	0.022	0.016	0.013	0.011	0.009	0.008	0.007
5	0.263	0.145	0.072	0.047	0.034	0.026	0.018	0.013	0.010	0.008	0.007	0.006	0.005
6	0.230	0.124	0.061	0.039	0.028	0.022	0.015	0.011	0.009	0.007	0.006	0.005	0.005
7	0.205	0.109	0.053	0.034	0.024	0.019	0.013	0.009	0.007	0.006	0.005	0.004	0.004
8	0.184	0.097	0.047	0.030	0.022	0.017	0.011	0.008	0.007	0.005	0.005	0.004	0.003
10	0.154	0.079	0.038	0.024	0.017	0.013	0.009	0.007	0.005	0.004	0.004	0.003	0.003
25	0.069	0.034	0.016	0.010	0.007	0.005	0.004	0.003	0.002	0.002	0.001	0.001	0.001
50	0.036	0.017	0.008	0.005	0.004	0.003	0.002	0.001	0.001	0.001	0.001	0.001	0.001
75	0.024	0.012	0.005	0.003	0.002	0.002	0.001	0.001	0.001	0.001	0.001	0.000	0.000
100	0.018	0.009	0.004	0.003	0.002	0.001	0.001	0.001	0.001	0.000	0.000	0.000	0.000

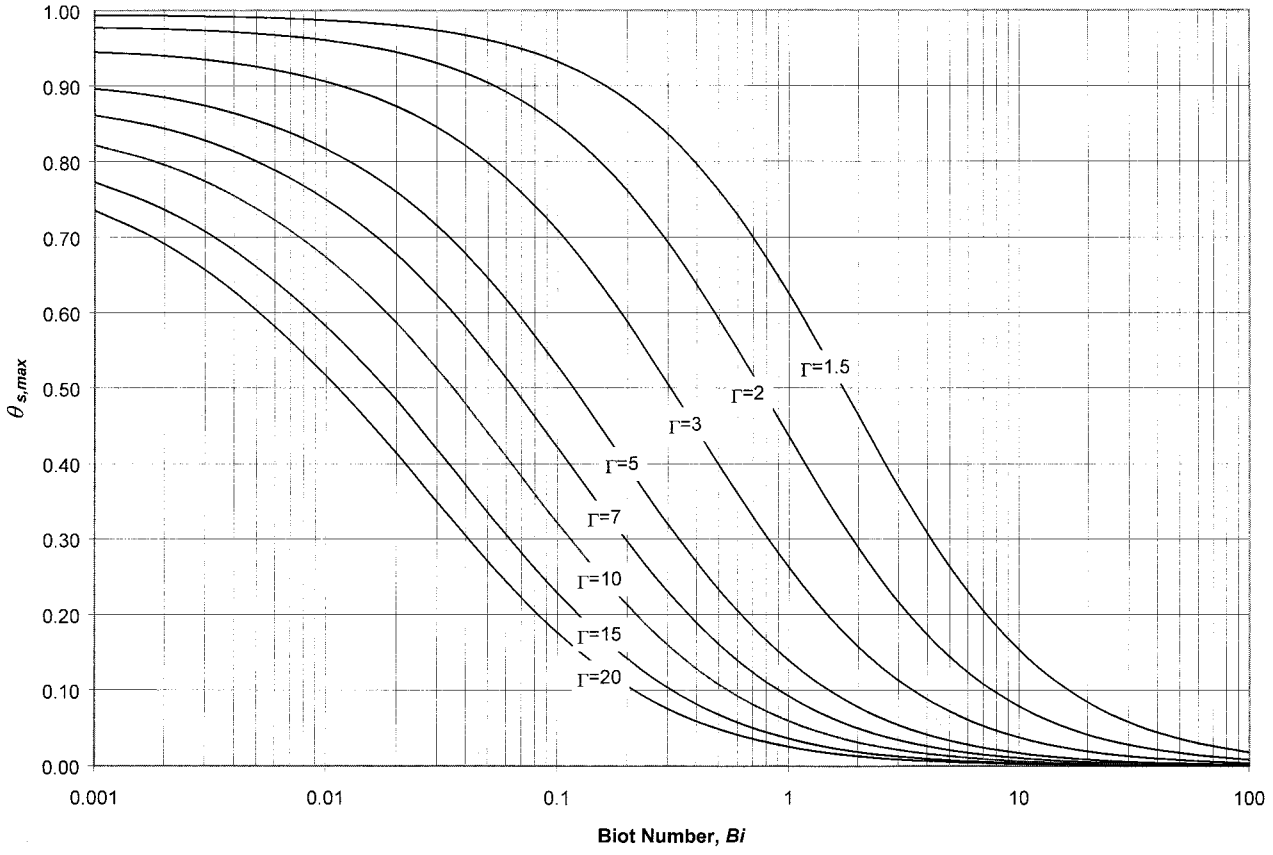

Fig. 8. Maximum surface temperature curves.

$$\theta(0,\psi) = -\frac{g(\psi)}{Bi}\left.\frac{\partial\theta}{\partial\phi}\right|_{\phi=0} = -\frac{g(\psi)}{Bi}\left(\frac{1-a_0}{\phi_0} - \Phi(\psi)\right). \tag{31}$$

All the quantities including the coefficient a_0 can be easily evaluated once $\Phi(\psi)$ is found.

Fig. 7 shows the effect of the Biot number on the surface temperature distribution. The surface temperature rise above the surrounding fluid temperature increases as the Biot number becomes smaller. Larger Biot numbers make the surface temperature more uniform and, as expected, the surface becomes an isotherm when the Biot number goes to infinity. Fig. 8 shows the maximum temperature on the exposed surface, which occurs directly above the center of the pipe, as a function of the Biot number and L/D. The maximum temperature is a strong function of both the Biot number and the geometrical parameter L/D. As the Biot number goes to zero, the maximum temperature approaches the pipe surface temperature. The maximum surface temperature is tabulated in Table 2.

3.4. Temperature distribution in the solid

The temperature field in the solid may be found by evaluating the series:

$$\theta(\phi,\psi) = a_0\left(1 - \frac{\phi}{\phi_0}\right) + \frac{\phi}{\phi_0} + \sum_{n=1}^{\infty} a_n \sinh\left[\lambda_n(\phi_0 - \phi)\right]\cos\ \lambda_n\psi \tag{32}$$

with the coefficients of the series obtained as a cosine series with a known surface temperature distribution, $\theta(0,\xi)$. The coefficients are simply

$$a_n = \frac{\int_0^1 \theta(0,\xi)\cos\ n\pi\xi\,\mathrm{d}\xi}{\sinh\ n\pi\phi_0}; \quad n = 1,2,\ldots \tag{33}$$

The following inverse transform relation is useful to express the temperature distribution in terms of physical coordinate system

$$F^{-1}(\zeta) = x + iy = \frac{i\sqrt{L^2 - a^2}(e^{\pi\zeta} - 1)}{e^{\pi\zeta} + 1}. \tag{34}$$

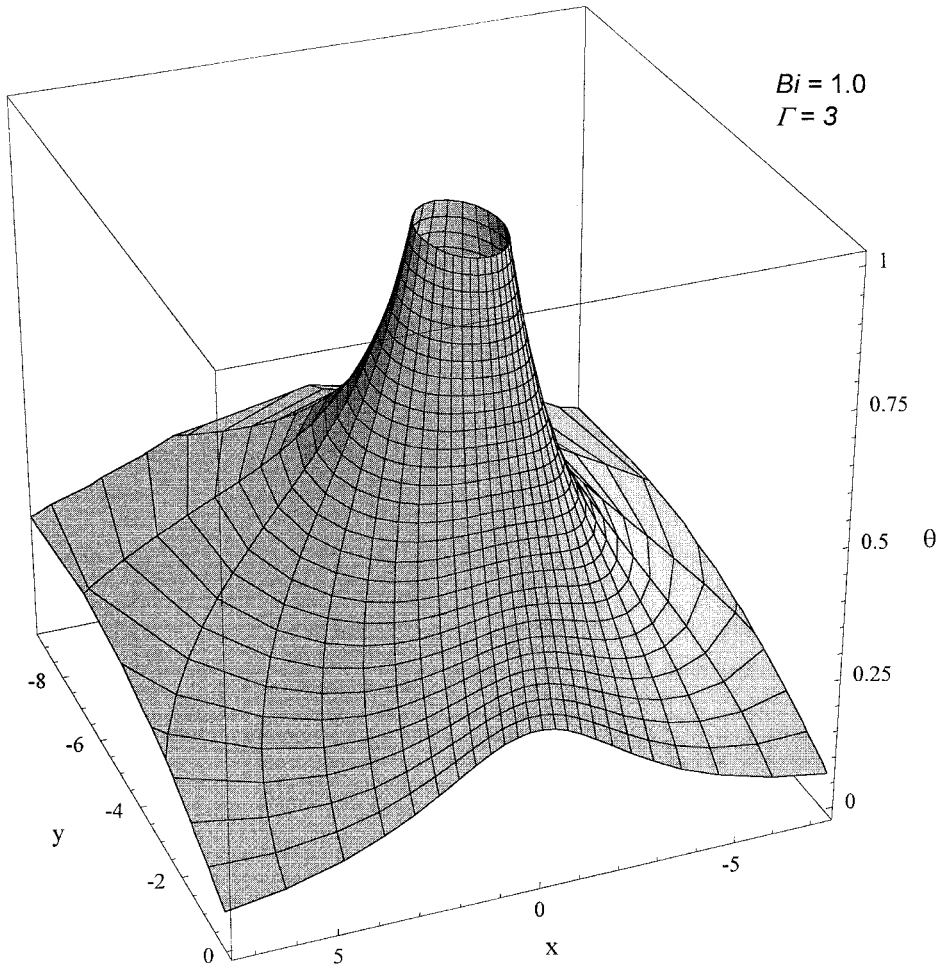

Fig. 9. Typical temperature distribution in solid.

A typical example of temperature distribution is shown in Fig. 9 in the physical coordinate system.

4. Conclusions

Conduction heat transfer from the isothermal surface of a buried circular tube is analyzed to investigate the effects of finite convective heat loss from the exposed ground surface. The original physical domain is transformed into a rectangular one through a conformal mapping and a singular integral equation is derived by imposing the convective heat transfer boundary condition for the exposed surface. This singular integral equation is then numerically solved to find the temperature distribution in the solid, and on the surface. The numerical scheme is efficient in the sense that it requires minimal computational efforts and it is robust in the sense that it does not give rise to any numerical problems such as divergence or instability. The total heat transfer rate from the pipe to the surrounding fluid is evaluated. The calculation results for the total heat transfer rate are presented by introducing the concept of panel efficiency that compares the actual heat transfer rate with the maximum possible one. Using a conventional shape factor, the heat transfer rate is cast into a useful form for design purposes. The panel efficiency and the maximum surface temperature are presented as functions of the Biot number and the geometrical parameter L/D. Both panel efficiency and maximum surface temperature are strong functions of these two nondimensional parameters implying that a constant surface temperature assumption can lead to significant calculation errors.

Acknowledgements

This study has been supported by grants from the Ministry of Education Korea, through Academic Research Program (Mechanical Engineering, Project No. ME97-A-12) while the first author was on sabbatical at the University of California, Irvine.

References

[1] I. Langmuir, E.Q. Adams, G.S. Meikle, Flow of heat through furnace walls: the shape factor, Trans. Am. Electrochem. Soc. 24 (1913) 53–81.
[2] J.E. Sunderland, K.R. Johnson, Shape factors for heat conduction through bodies with isothermal or convective boundary conditions, ASHRAE Trans. 70 (1964) 237–241.
[3] E. Hahne, U. Grigull, Shape factor and shape resistance for steady multi-dimensional heat conduction, Int. J. Heat Mass Transfer 18 (1975) 751–767.
[4] A. Bejan, in: Heat Transfer, 1st Ed., Wiley, New York, 1993, pp. 115–120.
[5] J.P. Holman, in: Heat Transfer, 7th Ed., McGraw-Hill, 1990, pp. 79–86.
[6] F.P. Incropera, D.P. DeWitt, in: Introduction to Heat Transfer, 3rd Ed., Wiley, New York, 1996, pp. 169–173.
[7] A.F. Mills, in: Heat and Mass Transfer, 1st Ed., Irwin, Chicago, 1995, pp. 142–147.
[8] Wolfram Research, in: E. Martin (Ed.), Mathematica 3.0 standard add-on packages, Cambridge University Press, 1996, pp. 147–148.
[9] F.B. Hildebrand, in: Advanced Calculus for Applications, 2nd Ed., Prentice-Hall, Englewood Cilffs, 1976, p. 205.
[10] D. Porter, D.S.G. Stirling, in: Integral Equations: A Practical Treatment from Spectral Theory to Applications, 1st Ed., Cambridge University Press, 1990, p. 3.
[11] K. Knopp, in: Infinite Sequences and Series, Dover Publication, New York, 1956, p. 171.
[12] I.S. Gradshteyn, I.M. Ryzhik, in: Tables of Integrals, Series, and Products, Academic Press, 1980, p. 38 (corrected and enlarged edn by A. Jeffrey) (1.441.2).
[13] W.H. Press, B.P. Flannery, S.A. Teukolsky, W.T. Vetterling, in: Numerical Recipes: The Art of Scientific Computing, 2nd Ed., Cambridge University Press, 1992, pp. 788–794.
[14] S. Wolfram, The Mathematica Book, Cambridge University Press, 1996.